RESEARCH PAPERS

Acta Cryst. (1998). B**54**, 705–713

Room-Temperature Superstructure of ZrV_2O_7

J. S. O. Evans,[a] J. C. Hanson[b] and A. W. Sleight[a]*

[a]*Department of Chemistry and Center for Advanced Materials, Oregon State University, Corvallis, Oregon, USA, and* [b]*Department of Chemistry, Brookhaven National Laboratory, Upton, New York, USA.*
E-mail: sleighta@chem.orst.edu

(*Received 27 May 1997; accepted 14 January 1998*)

Abstract

The structure of ZrV_2O_7, zirconium pyrovanadate, has been refined from single-crystal synchrotron X-ray data. As with other phases in the AM_2O_7 family, ZrV_2O_7 shows a set of strong reflections, which can be explained on the basis of a cubic unit cell with a = 8.765 Å, and a family of much weaker reflections due to a 3 × 3 × 3 superstructure. The superstructure has been refined to R_F = 0.036 (a = 26.296 Å, $Pa\bar{3}$, 6972 reflections) and contains highly regular ZrO_6 and VO_4 polyhedra. Of the six unique V_2O_7 groups, two are constrained by symmetry to contain linear V—O—V linkages, while the remaining four are free to bend away from 180°. The structural distortions from the ideal high-symmetry structure to the observed room-temperature structure are described.

1. Introduction

The structure of the aristotype of the cubic AM_2O_7 phases (ZrP_2O_7) was initially described by Levi & Peyronel (1935) using a simple cubic unit cell of dimension a = 8.2 Å and space group $Pa\bar{3}$. The first structural report of ZrV_2O_7 appeared some seven years later (Peyronel, 1942). The basic structure consists of corner-sharing AO_6 octahedra and MO_4 tetrahedra (Fig. 1). Each oxygen of an AO_6 octahedron is shared with an MO_4 tetrahedron. Each MO_4 tetrahedron shares three of its four O atoms with an AO_6 octahedron, whilst the fourth is shared with another MO_4 tetrahedron leading to an M_2O_7 pyrophosphate or pyrovanadate group. The structure can be thought of as related to the face-centered cubic structure of NaCl, with AO_6 groups centered at the ideal Na sites and the bridging oxygen of the M_2O_7 groups at the Cl site. The symmetry of the M_2O_7 groups necessarily lowers the overall symmetry from $Fm\bar{3}m$ to $Pa\bar{3}$. In the ideal structure the bridging O atom of the M_2O_7 group lies on a $\bar{3}$ site and the A—O—A angle is therefore constrained to be 180°.

Several workers realized that the linear M—O—M bonds required by the cubic structure of ZrV_2O_7 are somewhat unusual and that in nearly all cases this simple model would require very short M—O bridging bond distances (*e.g.* for ZrV_2O_7 a bridging bond distance of 1.46 Å would be required). These structural inconsistencies are clearly reminiscent of those encountered in the more familiar controversy surrounding the crystallochemically implausible Si—O distances which must be inferred when assuming the ideal (*C*9) structure for β-cristobalite.

A potential explanation for this apparent inconsistency came in 1963 when Völlenke *et al.* (1963) reported evidence for a $3a \times 3a \times 3a$ supercell in single-crystal X-ray photographs of GeP_2O_7. This observation suggested that the apparent linearity of the M—O—M bond was an artifact owing to the missed superlattice. Refinement of the average position of bent M_2O_7 groups in each of the 27 'subcells' of the true superstructure leads to an overall disordered atomic arrangement and an apparent linearity of the M_2O_7 groups.

Subsequently, evidence of similar supercells has been reported for a number of AM_2O_7 phases, including SiP_2O_7 (Völlenke *et al.*, 1963; Hagmann & Kierkegaard, 1969; Liebau *et al.*, 1968), TiP_2O_7 (Völlenke *et al.*, 1963; Norby, 1996; Sanz *et al.*, 1997), ZrP_2O_7 (Hagmann & Kierkegaard, 1969; Chaunac, 1971; Pascard *et al.*, 1971; Khosrovani & Sleight, 1996), SnP_2O_7 (Völlenke *et al.*, 1963; Huang *et al.*, 1975), CeP_2O_7 (Völlenke *et al.*, 1963), HfP_2O_7 (Völlenke *et al.*, 1963), ReP_2O_7 (Banks & Sacks, 1982), PbV_2O_7 (Völlenke *et al.*, 1963), ThP_2O_7 (Burdese & Borlera, 1963), UP_2O_7 (Burdese & Borlera, 1960), MoP_2O_7 (Haushalter & Mundi, 1992) and ZrV_2O_7 (Korthuis *et al.*, 1995; Khosrovani *et al.*, 1997). However, for cases where powder X-ray data on samples which are not 100% pure are the only evidence, the existence of a true commensurate 3 × 3 × 3 superlattice cannot be considered definitive (A = Ce, Th, U, Pb, Re). Related phases continue to be reported with the simple cubic cell and it is difficult to know whether these represent true examples of simple cubic systems or whether the superlattice was too weak to be observed by the authors. Examples in this category include $Ta_{1-x}P_{1.8+x}O_7$ (Oyetola *et al.*, 1991) and $AA'P_2O_7$ (A/A' = Bi/Ta, Sb/Ta,

Bi/Nb, Nd/Ta, Eu/Nb, Eu/Ta; Oyetola *et al.*, 1991). In the case of NbP_2O_7 the superstructure in a reduced Nb^{IV} sample observed in electron diffraction experiments is not observed for oxidized Nb^{V}-containing samples (Fukuoka *et al.*, 1995; Oyetola *et al.*, 1991; Zah Letho *et al.*, 1994). We are unaware of good evidence for superlattice reflections in the isostructural arsenates (A = Th, U).

There has been, to our knowledge, only one published attempt at the single-crystal structure solution of the superstructure of these materials, that of SiP_2O_7 by Tillmanns *et al.* (1973), which used a combination of X-ray diffraction data and distance least-squares (DLS) modeling to describe the structure. While a 'tour de force' in its day, computational limitations and the relatively poor data available restricted the authors to an isotropic refinement model.

There has been considerable interest in the negative thermal expansion properties of ZrV_2O_7 and recent papers have described work on the structure and properties of the $ZrV_{2-x}P_xO_7$ series using a combination of diffraction and spectroscopic techniques (Korthuis *et al.*, 1995; Khosrovani & Sleight, 1996; Hudalla *et al.*, 1996). In particular, powder neutron diffraction techniques have been used to try to understand the details of the superstructure and the phase changes observed on warming the sample. Owing to the complexity of the problem (ZrV_2O_7 has 50 atoms in the asymmetric unit) and the weak nature of the superlattice reflections (the strongest calculated superlattice reflection is ~1% of the strongest subcell peak in both X-ray and neutron diffraction patterns), an accurate structure is not possible from powder data.

We were interested in addressing a number of questions concerning the structure and phase transitions of ZrV_2O_7. Firstly, determining the true symmetry of the room-temperature structure was especially important because, unlike the AP_2O_7 cubic phases, ZrV_2O_7 has two phase transitions above room temperature. Secondly, we wanted to be able to describe the precise nature of the polyhedral tilts and/or distortions which lead to the superstructure formation. In this work we report the single-crystal X-ray structure of ZrV_2O_7 using data collected at beamline X7B of the National Synchrotron Light Source (NSLS). Temperature-dependent studies including structure refinements at both 363 and 375 K have also been performed and suggest a simple model for the observed thermal expansion behavior. At 345 K, however, an incommensurate superlattice phase is formed. These experiments are the subject of another publication (Withers *et al.*, 1998).

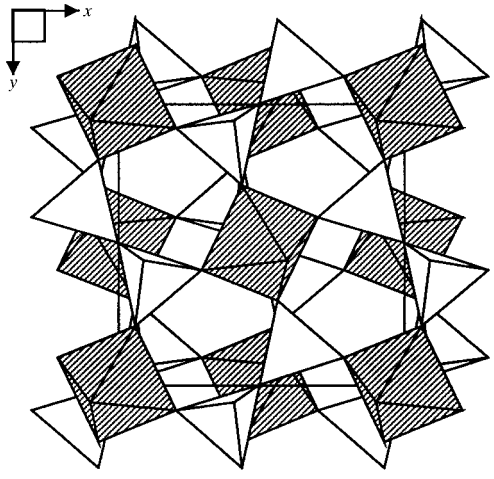

Fig. 1. Ideal cubic structure of ZrV_2O_7. ZrO_6 octahedra are shaded, V_2O_7 groups are unshaded.

2. Experimental

ZrV_2O_7 melts incongruently to ZrO_2 and a liquid at a temperature reported to be 1020 K (Burdese & Borlera, 1960) or 1113 K (Buchanan & Walter, 1983). Single crystals were grown from a V_2O_5-rich melt. Reagents were heated to 1123 K in a platinum crucible, then cooled at 2 K h^{-1} to 1023 K and then at 10 K h^{-1} to room temperature. An approximately cubic crystal was mounted on a glass fiber for data collection. Preliminary precession photographs confirmed the presence of a $3a \times 3a \times 3a$ superstructure. Full experimental details are given in Table 1.

Data were collected using a Fuji image plate system on beamline X7B of the NSLS with wavelength 1.088 Å (calibrated with an LaB_6 standard). Using a 2θ film offset of 0°, data were collected with 4° rotation intervals (2000 steps per degree) over a 180° angular range. Two data sets were collected at a scan speed of 0.01° s^{-1} and a scan speed of 0.025° s^{-1} to increase the effective dynamic range of the image plates. A third set of images was collected over a 90° range with image plates at 2θ = 40°, using a rotation range of 3° per image and a scan speed of 0.01° s^{-1}.

Digitized image plates were indexed, integrated, scaled and merged using the *DENZO* and *SCALEPACK* software packages (Otwinowski, 1993; Minor, 1993). For final refinements data over the rotation range 0–90° were used (76 images in total). No absorption correction was applied. A total of 77 208 measured reflections were merged to 10 158 unique reflections with an overall R_{merge} of 0.058 (based on I). Of these, 2440 reflections were measured once only, 2393 twice only. Of the 10 158 unique reflections, 9456 were observed to have $I > 0$ and 6972 had $I > 3\sigma(I)$. Some 6647 of these are 'superlattice' reflections. Various other intensity sets were prepared to check refinement results: sets using/excluding the strongest/weakest reflections and sets using only reflections measured at least two or three times. These are discussed in the main body of the text. The F^2 and $\sigma(F^2)$ values were then rescaled to an F8.2 format and subsequent refinement was carried out

within the Oxford *CRYSTALS* suite of programs (Watkin *et al.*, 1985). Distance least-squares calculations were performed using both *DLS*-76 (Baerlocher *et al.*, 1977) and *CRYSTALS* (Watkin *et al.*, 1985). Polyhedral tilt angles were derived by least-squares fitting of an octahedron with fixed 90° bond angles, but with an overall $M-$O distance allowed to refine, within the *GSAS* suite of programs (Larson & Von Dreele, 1994).

The cubic cell edge of the room-temperature phase was obtained from a number of sources. Refinement of the cell edge within the *DENZO* program suite gave 26.296 Å. Least-squares refinement of the position of 25 high-angle ($2\theta > 45°$) subcell reflections accurately centered on a Rigaku AFC-6*R* diffractometer using Mo $K\alpha$ (λ = 0.71069 Å) radiation gave a cell edge of 26.2988 (9) Å. Least-squares refinement of the position of 20 sub- and supercell reflections of a powdered sample of ZrV_2O_7 collected on beamline X7A of the NSLS gave a cell edge of 26.3082 (2) Å. Bond distances and angles reported are based on the cell edge of 26.296 Å.

3. Structure refinement

Analysis of the images obtained suggested that all reflections could be indexed on a cubic cell with a = 26.296 Å. No evidence of any metric lowering of symmetry was obtained. Systematic absences ($0kl$, $k = 2n$) suggested the space group $Pa\bar{3}$. Some very weak violations of these extinction conditions were observed and of the 361 $0kl$ reflections with $I > 3\sigma(I)$ recorded, some 21 reflections were 'observed' with k = odd. However, all these reflections were relatively weak [the strongest 'violation' ranked 4425 of the 6972 reflections with $I > 3\sigma(I)$ measured and was only 1.3% of the intensity of the strongest superlattice reflection or ~0.02% of the strongest sublattice reflection; 19 of the 21 violations ranked below 6200, *i.e.* < 0.4% of the strongest superlattice reflection] and also showed considerable scatter in the intensities measured on individual images. These reflections were also all subcell reflections (*i.e.* $h, k, l = 3n$) and could arise from multiple diffraction effects. Separate scaling then merging of Friedel pairs indicated no significant anomalous signal, which could indicate a reduction of symmetry to noncentrosymmetric $P2_13$. Thus, the space groups of the room- and high-temperature (> 375 K) ideal ZrV_2O_7 structures are identical and, in fact, the maximal isomorphic subgroup of $Pa\bar{3}$ is $Pa\bar{3}$ ($a' = 3a$, $b' = 3b$, $c' = 3c$). The transition from the high- to the low-temperature structure preserves the point group, but destroys 26/27 of the translational symmetry elements and two-thirds of the threefold axes.

Approximate starting coordinates for structure refinement were obtained from previous powder work (Khosrovani *et al.*, 1997). Least-squares refinement (anisotropic displacement parameters, 407 variables) of the full data set using unit weights led rapidly to an R factor of R_F = 0.0431, wR_F = 0.0525, suggesting an essentially correct structural model. Comparison of F_{obs} and F_{calc} suggested some systematic errors, with the strongest reflections significantly overestimated. Application of a third-order Chebychev polynomial weighting scheme could correct for these errors and led to a final R factor of R_F = 0.0360, wR_F = 0.0414. Such a systematic error is to be expected. Owing to the high intensity of the subcell reflections relative to the supercell reflections, even at the faster scan speed used at $2\theta = 0°$ and on the high-angle $2\theta = 40°$ images, several of the strongest subcell peaks remained saturated.

Table 1. *Experimental details*

Crystal data	
Chemical formula	ZrV_2O_7
Chemical formula weight	305.0988
Cell setting	Cubic
Space group	$Pa\bar{3}$
a (Å)	26.296
V (Å^3)	18183.15
Z	108
D_x (Mg m^{-3})	3.009
Radiation type	Synchrotron
Wavelength (Å)	1.088
μ (mm^{-1})	4.11
Temperature (K)	298
Crystal form	Cubic
Crystal size (mm)	0.1 × 0.1 × 0.1
Crystal color	Orange
Data collection	
Diffractometer	Fuji image plate system
Data collection method	φ scans
Absorption correction	None
No. of measured reflections	77 208
No. of independent reflections	10 158
No. of observed reflections	6972
Criterion for observed reflections	$I > 3\sigma(I)$
R_{int}	0.058
Range of h, k, l	$0 \rightarrow h \rightarrow 27$ $0 \rightarrow k \rightarrow 28$ $1 \rightarrow l \rightarrow 39$
Refinement	
Refinement on	F
R	0.0366
wR	0.0414
S	0.905
No. of reflections used in refinement	6972
No. of parameters used	407
Weighting scheme	Third-order Chebyshev polynomial, coefficients 0.280, 0.245, 0.056
$(\Delta/\sigma)_{max}$	0
$\Delta\rho_{max}$ (e Å^{-3})	1.00
$\Delta\rho_{min}$ (e Å^{-3})	−2.39
Extinction method	Larson (1970) (equation 22)
Source of atomic scattering factors	*International Tables for X-ray Crystallography* (1974, Vol. IV, Table 2.2*B*)

Table 2. *Fractional atomic coordinates and equivalent isotropic displacement parameters (Å^2)*

$U_{eq} = (1/3)\Sigma_i\Sigma_j U^{ij} a^i a^j \mathbf{a}_i.\mathbf{a}_j$.

	x	*y*	*z*	U_{eq}
Zr(1)	0.497434 (8)	−0.001114 (8)	0.165602 (8)	0.0063
Zr(2)	0.500084 (8)	0.32661 (1)	0.164329 (9)	0.0061
Zr(3)	0.496217 (8)	0.170143 (9)	0.34384 (1)	0.0054
Zr(4)	0.331355 (8)	0.162024 (9)	0.166102 (8)	0.0064
Zr(5)	0.334645 (8)	0.334645 (8)	0.334645 (8)	0.0068
Zr(6)	1/2	1/2	0	0.0064
V(1)	0.46207 (2)	0.12653 (2)	0.13145 (2)	0.0099
V(2)	0.47030 (2)	0.45683 (2)	0.12993 (2)	0.0094
V(3)	0.36952 (2)	0.29152 (2)	0.12774 (2)	0.0094
V(4)	0.29521 (2)	0.36857 (2)	0.20539 (2)	0.0096
V(5)	0.30164 (2)	0.12878 (2)	0.03361 (2)	0.0086
V(6)	0.37478 (2)	0.21139 (2)	−0.03950 (2)	0.0097
V(7)	0.53727 (2)	0.54143 (2)	0.20594 (2)	0.0096
V(8)	0.53403 (2)	0.20035 (2)	0.21313 (2)	0.0092
V(9)	0.20147 (2)	0.20147 (2)	0.20147 (2)	0.0103
V(10)	0.53834 (2)	−0.03834 (2)	0.03834 (2)	0.0087
V(11)	0.12459 (2)	0.12459 (2)	0.12459 (2)	0.0093
O(11)	0.48004 (8)	0.06539 (8)	0.12620 (8)	0.0193
O(12)	0.40009 (8)	0.12892 (9)	0.14660 (9)	0.0237
O(13)	0.47258 (9)	0.15725 (8)	0.07648 (8)	0.0197
O(21)	0.49048 (8)	0.39627 (8)	0.12804 (8)	0.0205
O(22)	0.4726 (1)	0.48128 (9)	0.07129 (8)	0.0231
O(23)	0.41032 (8)	0.45904 (8)	0.15181 (9)	0.0202
O(31)	0.3524 (1)	0.3083 (1)	0.06917 (9)	0.0259
O(32)	0.3565 (1)	0.22994 (9)	0.1359 (1)	0.0281
O(33)	0.43193 (8)	0.3013 (1)	0.13571 (9)	0.0242
O(41)	0.23557 (8)	0.36060 (9)	0.18436 (9)	0.0238
O(42)	0.3133 (1)	0.42848 (9)	0.1951 (1)	0.0257
O(43)	0.29834 (9)	0.35604 (9)	0.26787 (8)	0.0232
O(51)	0.30180 (9)	0.14271 (9)	0.09573 (8)	0.0227
O(52)	0.24174 (8)	0.12759 (9)	0.01154 (9)	0.0209
O(53)	0.32893 (8)	0.07216 (8)	0.02455 (9)	0.0214
O(61)	0.35597 (8)	0.27237 (8)	−0.03702 (8)	0.0201
O(62)	0.43498 (8)	0.20653 (8)	−0.01851 (9)	0.0218
O(63)	0.37015 (9)	0.18931 (9)	−0.09934 (8)	0.0229
O(71)	0.52060 (9)	0.53508 (8)	0.26734 (8)	0.0221
O(72)	0.51715 (9)	0.59745 (8)	0.18395 (9)	0.0237
O(73)	0.60074 (8)	0.53739 (9)	0.20051 (9)	0.0229
O(81)	0.51072 (9)	0.25854 (8)	0.20207 (9)	0.0231
O(82)	0.59407 (8)	0.19718 (9)	0.19242 (9)	0.0229
O(83)	0.53230 (9)	0.18804 (9)	0.27580 (8)	0.0234
O(91)	0.26222 (8)	0.1951 (1)	0.18376 (9)	0.0248
O(101)	0.59815 (8)	−0.01624 (8)	0.03707 (8)	0.0194
O(111)	0.06452 (8)	0.14578 (9)	0.12622 (9)	0.0217
O(108)	0.4973 (10)	0.1550 (1)	0.1807 (1)	0.0307
O(207)	0.5101 (1)	0.4920 (1)	0.1707 (1)	0.0323
O(304)	0.3362 (1)	0.3271 (1)	0.1730 (1)	0.0363
O(506)	0.3357 (1)	0.1759 (1)	0.0004 (1)	0.0335
O(911)	0.16284 (9)	0.16284 (9)	0.16284 (9)	0.0360
O(1010)	1/2	0	0	0.0361

To verify these effects, refinement was also performed with the 300 most intense reflections excluded from the data set. Using unit weights an agreement factor of R_F = 0.0366 (6641 reflections) was obtained (*cf.* 0.0360 using all data). Atomic shifts between these two models of refinement were small (average shift 0.005 Å; maximum shift 0.010 Å). Refinements were also performed using just reflections which had been recorded at least two or at least three times. The greater redundancy of such data sets can be expected to yield better average intensity data. Reflections measured ≥ 2 times yielded an overall agreement factor of R_F = 0.0337, wR_F = 0.0397 [5586 reflections with $I > 3\sigma(I)$]; for reflections measured ≥ 3 times R_F = 0.0328, wR_F = 0.0351 [4067 reflections with $I > 3\sigma(I)$]. Average atomic shifts between all these refinements were small (< 0.01 Å). We choose to report here results based on the weighted refinement of all data, as the larger number of reflections (particularly at high angles where redundancy is lowest) can be expected to yield a more accurate refined model. Final atomic coordinates and displacement parameters are reported in Table 2, distances and angles in Table 3.† We emphasize that such a model gives good agreement with both subcell and supercell reflections. With a fixed scale factor and a unit weighting scheme R_F values are 0.0413, 0.0466 and 0.0540 for all, subcell only (h, k, $l = 3n$) and supercell reflections, respectively.

A view of a section of the refined structure of ZrV_2O_7 is shown in Fig. 2, along with a view of the ideal undistorted structure. The structure of the room-temperature form of ZrV_2O_7 is closely related to that of the ideal high-temperature form. Indeed, the room-temperature structure can be readily derived from the high-temperature form *via* a three-dimensionally coupled rotation of the polyhedral building blocks of the framework structure. The loss of symmetry elements associated with this transition is such that whilst the high-temperature structure contains one Zr atom and one V atom in the asymmetric unit, the room-temperature structure contains six unique Zr sites and 11 V. Of the 11 V atoms, three (V9, V10 and V11) lie on the threefold axis. Of the six unique V_2O_7 groups in the cell (O1010 in the structure lies on an inversion center; V10—O1010—V10 therefore forms a V_2O_7 group) two are therefore constrained by symmetry to have V—O—V 180° bridging bond angles. The remaining four groups, however, can bend away from 180°, leading to an overall volume decrease in the structure. Bridging bond angles (Table 3, Fig. 3) of 159.3, 162.9, 166.2 and 167.6° result.

This coupled rotation of the polyhedral building blocks also leads to a range of Zr—O—V bond angles. In the ideal high-symmetry structure the single Zr—O—V bond angle would be expected to be 163° (derived from DLS refinements using experimentally determined average Zr—O and V—O distances); in the room-temperature structure the 27 unique Zr—O—V bond angles range from 145 to 174° (average = 158°, standard uncertainty of the individual angles 6.3°), see Fig. 4.

Individual metal–oxygen distances in the structure show a remarkably narrow range of values. The average Zr—O bond distance is 2.0695 Å with a standard

† Supplementary data for this paper are available from the IUCr electronic archives (Reference: CR0528). Services for accessing these data are described at the back of the journal.

Table 3. *Selected geometric parameters (Å, °)*

Zr(1)—O(11)	2.084 (2)	V(3)—O(31)	1.665 (2)
Zr(1)—O(13)	2.075 (2)	V(3)—O(32)	1.669 (2)
Zr(1)—O(53)	2.083 (2)	V(3)—O(33)	1.674 (2)
Zr(1)—O(62)	2.071 (2)	V(4)—O(41)	1.676 (2)
Zr(1)—O(71)	2.059 (2)	V(4)—O(42)	1.668 (2)
Zr(1)—O(101)	2.070 (2)	V(4)—O(43)	1.678 (2)
Zr(2)—O(21)	2.081 (2)	V(5)—O(51)	1.674 (2)
Zr(2)—O(31)	2.068 (2)	V(5)—O(52)	1.679 (2)
Zr(2)—O(33)	2.055 (2)	V(5)—O(53)	1.670 (2)
Zr(2)—O(61)	2.078 (2)	V(6)—O(61)	1.679 (2)
Zr(2)—O(73)	2.066 (2)	V(6)—O(62)	1.681 (2)
Zr(2)—O(81)	2.066 (2)	V(6)—O(63)	1.682 (2)
Zr(3)—O(23)	2.060 (2)	V(7)—O(71)	1.681 (2)
Zr(3)—O(42)	2.061 (2)	V(7)—O(72)	1.669 (2)
Zr(3)—O(52)	2.067 (2)	V(7)—O(73)	1.678 (2)
Zr(3)—O(72)	2.076 (2)	V(8)—O(81)	1.674 (2)
Zr(3)—O(83)	2.079 (2)	V(8)—O(82)	1.672 (2)
Zr(3)—O(111)	2.063 (2)	V(8)—O(83)	1.680 (2)
Zr(4)—O(12)	2.071 (2)	V(9)—O(91) × 3	1.672 (2)
Zr(4)—O(32)	2.063 (2)	V(10)—O(101) × 3	1.677 (2)
Zr(4)—O(41)	2.067 (2)	V(11)—O(111) × 3	1.676 (2)
Zr(4)—O(51)	2.070 (2)	V(1)—O(108)	1.761 (2)
Zr(4)—O(82)	2.062 (2)	V(8)—O(108)	1.755 (2)
Zr(4)—O(91)	2.068 (2)	V(2)—O(207)	1.762 (2)
Zr(5)—O(43) × 3	2.076 (2)	V(7)—O(207)	1.748 (2)
Zr(5)—O(63) × 3	2.069 (2)	V(3)—O(304)	1.749 (2)
Zr(6)—O(22) × 6	2.068 (2)	V(4)—O(304)	1.754 (2)
V(1)—O(11)	1.681 (2)	V(5)—O(506)	1.761 (3)
V(1)—O(12)	1.679 (2)	V(6)—O(506)	1.740 (3)
V(1)—O(13)	1.679 (2)	V(9)—O(911)	1.759 (4)
V(2)—O(22)	1.672 (2)	V(11)—O(911)	1.742 (4)
V(2)—O(23)	1.680 (2)	V(10)—O(1010) × 2	1.7460 (7)
Zr(1)—O(11)—V(1)	145.4 (1)	Zr(5)—O(63)—V(6)	157.3 (1)
Zr(4)—O(12)—V(1)	157.2 (1)	Zr(1)—O(71)—V(7)	158.2 (1)
Zr(1)—O(13)—V(1)	155.8 (1)	Zr(3)—O(72)—V(7)	171.3 (2)
Zr(2)—O(21)—V(2)	149.3 (1)	Zr(2)—O(73)—V(7)	149.8 (1)
Zr(6)—O(22)—V(2)	160.1 (2)	Zr(2)—O(81)—V(8)	157.7 (1)
Zr(3)—O(23)—V(2)	153.3 (1)	Zr(4)—O(82)—V(8)	159.5 (2)
Zr(2)—O(31)—V(3)	173.7 (2)	Zr(3)—O(83)—V(8)	154.2 (1)
Zr(4)—O(32)—V(3)	162.8 (2)	Zr(3)—O(111)—V(11)	159.0 (1)
Zr(2)—O(33)—V(3)	161.9 (1)	Zr(4)—O(91)—V(9)	160.8 (2)
Zr(4)—O(41)—V(4)	165.3 (2)	Zr(1)—O(101)—V(10)	153.6 (1)
Zr(3)—O(42)—V(4)	168.3 (2)	V(1)—O(108)—V(8)	159.3 (2)
Zr(5)—O(43)—V(4)	154.7 (1)	V(2)—O(207)—V(7)	162.9 (2)
Zr(4)—O(51)—V(5)	157.9 (1)	V(3)—O(304)—V(4)	166.2 (2)
Zr(3)—O(52)—V(5)	156.2 (1)	V(5)—O(506)—V(6)	167.6 (2)
Zr(1)—O(53)—V(5)	156.5 (1)	V(9)—O(911)—V(11)	180
Zr(2)—O(61)—V(6)	153.2 (1)	V(10)—O(101)—V(10)	180
Zr(1)—O(62)—V(6)	153.0 (1)		

uncertainty of the 27 values of 0.0075 Å (*cf.* a typical experimental s.u. on an individual distance of 0.002 Å) and a range of only 2.055–2.084 Å. The average $V—O_{Zr}$ (*i.e.* a V—O distance of a V—O—Zr linkage) is 1.6757 Å with a standard uncertainty in the 27 values of 0.0046 Å and a range of 1.665–1.682 Å. Internal bond angles of the ZrO_6 and VO_4 polyhedra show minimal departure from ideal octahedral and tetrahedral values. The 72 ZrO_6 90° angles show a range of 88.0–92.0° with a standard uncertainty of 1°. The 66 VO_4 tetrahedral bond angles show a range of 108.3–110.6° with a standard uncertainty of 0.47°. The difference between tetrahedral angles involving bridging O atoms (*i.e.* $O_V—V—O_{Zr}$) and nonbridging O atoms (*i.e.* $O_{Zr}—V—O_{Zr}$) is small, averages being 109.3 (5)° (18 bond angles) and 109.5 (5)° (48 bond angles), respectively.

The dependence of both Zr—O and $V—O_{Zr}$ distances on the Zr—O—V angle is small. Fig. 4 shows the dependence of V—Zr nonbonded distances on the angle of the Zr—O—V bond. The 27 such distances agree well with predicted values derived from overall average bond distances (using average Zr—O and V—O distances, the

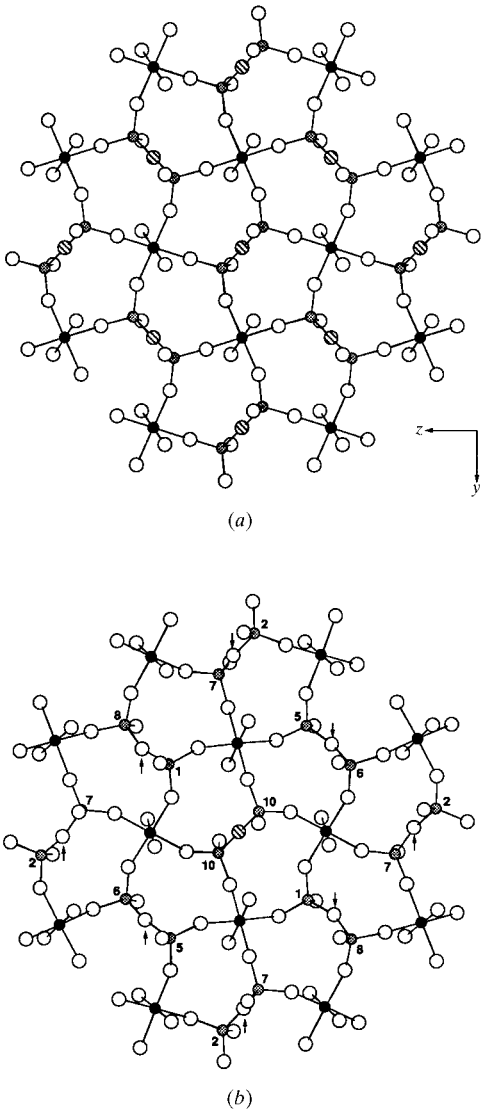

Fig. 2. View down [100] of (*a*) a section of the ideal (high-temperature) structure of ZrV_2O_7 and (*b*) the distorted room-temperature structure; Zr as black circles, V as shaded circles, O as either open (general position) or cross-hatched (threefold axis) circles. In the ideal structure all bridging V—O—V angles are constrained by symmetry to be 180°. In the room-temperature structure arrowed bonds can distort to a more favorable arrangement. The V-atom numbering scheme is shown.

experimentally determined bond angle and simple geometrical arguments). This suggests that the Zr—O—V bridges can be viewed as ideally flexible and little distortion of individual bond distances occurs as the bond is bent.

The $V—O_V$ bridging bonds of the V_2O_7 units are systematically longer than the $V—O_{Zr}$ bonds with an average distance of 1.7525 Å and standard uncertainty of 0.0076 Å. The overall range found for the 11 unique distances is 1.740–1.762 Å. Fig. 5(*a*) shows how the V—V distance of each V—O—V linkage depends on the observed bond angle. The trend observed clearly shows that the $V—O_V$ distance is correlated with the bridging bond angle, with linear bonds being somewhat shorter than bent bonds. Similar effects have been observed in silicates where the Si—O bond distance has been calculated to vary between 1.638 and 1.596 Å as the bond angle changes from 120 to 180° (Gibbs *et al.*, 1994). The origin of this effect, even in silicates, remains controversial, with some authors invoking increased *d*-orbital π-bonding contributions as the bond angle approaches 180°. The 3*d* orbitals are much more likely to be relevant to bonding in vanadates; thus, an even greater shortening of the V—O bond might be anticipated as the V—O—V bond angle approaches 180°. Fig. 6 shows data taken from 17 of the 20 structural refinements of $M_2V_2O_7$ compounds reported (M = Cu, Mg, Co, Ni, Hg, Zn, Pb, Sr, Ca, Cd, Ba). The three structures available in the ICSD omitted from this plot each showed chemically implausible bond distances/calculated atomic valences. There is again an overall decrease in the $V—O_V$ distance as a function of increasing bond angle. Clearly the direct comparison of these two curves is not completely justified as the $M_2V_2O_7$ structures will contain other structure-directing interactions (*e.g.* bonding interactions directly between the bridging O atom and M cations which are not present in the framework ZrV_2O_7 structure). It is interesting to note, nonetheless, that the extrapolated 180° value of this line of d = 1.744 Å is very close to the average value observed for the two 180° V_2O_7 groups of ZrV_2O_7 (1.7525 Å). Data from the current refinement are included in Fig. 6 for comparison.

There is some question as to whether these effects are merely an artifact of enhanced thermal motion in the bridging O atoms of the threefold V_2O_7 groups. Analysis of equivalent displacement parameters of the O atoms in the structure suggests that V—O—V O atoms do have larger displacement parameters than Zr—O—V O atoms [V—O—V average U_{eq} = 0.034 (2); Zr—O—V average U_{eq} = 0.023 (3) Å^2]. The displacement parameters of the threefold O atoms (both values = 0.036 Å^2) are not, however, significantly different from other V—O—V O atoms. The magnitude of the displacement ellipsoid of these threefold O atoms corresponds to an r.m.s. displacement of approximately 0.24 Å perpendicular to the threefold axis. It is therefore difficult to conclude from diffraction data alone whether or not the threefold V—O—V groups truly contain 180° bonds. For a V—V distance of 3.5 Å a static displacement of this magnitude would result in a bond angle of approximately 164°. A recent combined NMR and powder X-ray study by Sanz *et al.* (1997) on TiP_2O_7 was interpreted in terms of static disorder around the threefold axis. The proximity of room-temperature ZrV_2O_7 to two displacive phase transitions might

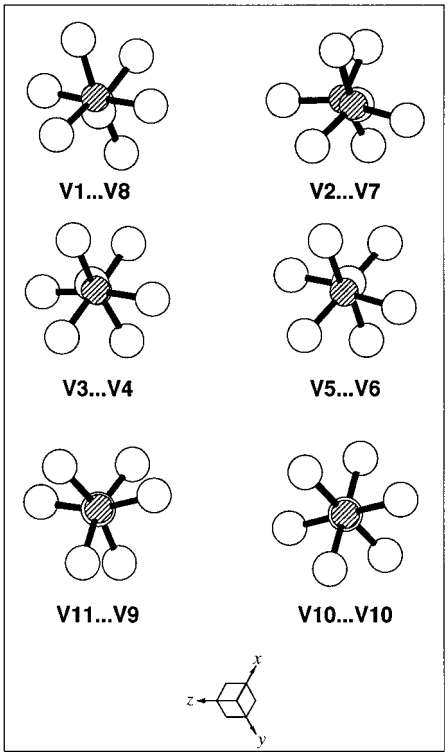

Fig. 3. Views of the six independent V_2O_7 groups along the threefold axis.

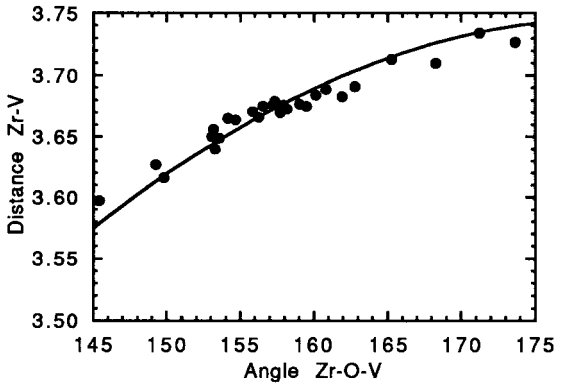

Fig. 4. Dependence of Zr—V distance on the Zr—O—V bond angle. The 27 observed distances are shown as points, whilst the calculated curve using experimentally determined average Zr—O and V—O distances is given as a full line.

Table 4. *Tilt angles (°) of the six unique ZrO_6 octahedra*

Values for all six polyhedra in an ideal untilted structure would be x tilt = −24.43°, y tilt = −15.88°, z tilt = −24.43°.

Octahedron	x tilt obs	y tilt obs	z tilt obs	x tilt calc	y tilt calc	z tilt calc
1	−30.712	−4.8560	−19.244	−30.670	−5.7180	−19.610
2	−30.714	−21.211	−20.434	−30.045	−20.469	−21.001
3	−22.413	−22.642	−20.176	−22.371	−21.872	−20.266
4	−23.666	−13.809	−25.736	−24.711	−14.184	−25.857
5	−28.280	−17.122	−28.280	−27.761	−16.970	−27.761
6	−20.279	−14.401	−20.279	−20.084	−14.115	−20.084

suggest dynamic disorder as being more likely in this case. However, given the complexity of V—O bonding and the recent description of correlations between bending vibrations and M—O bond distances in these structures (Seo & Whangbo, 1997), we do not feel that the current data permit firm conclusions as to the true nature of this bond. It is clear, however, that the phase transition from the simple cubic high-temperature structure, which allows the ordered distortion of four of the six V_2O_7 groups to a more favorable geometry, does not relieve the frustration of the remaining two.

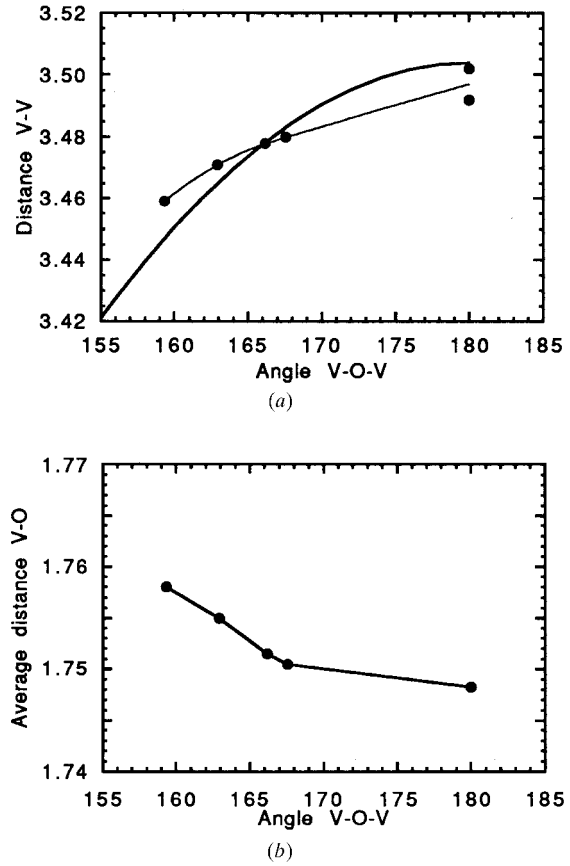

Fig. 5. (*a*) Dependence of V—V distance on the V—O—V bond angle. Observed data shown as joined points, calculated distances based on average V—O_V distances as a heavy line. (*b*) Dependence of average V—O_V distance on V—O—V bond angle for the six independent V_2O_7 groups.

Given the complexity of the room-temperature structure of ZrV_2O_7, the magnitudes of the room-temperature distortions are most readily visualized by considering the polyhedra of the structure rather than individual atomic shifts. Table 4 shows the experimentally observed tilt angles of the six individual ZrO_6 octahedra. Tilt angles are defined as the angle that a regular MO_6 octahedron would have to be tilted around the z, y and x axes to achieve the least-squares fit to the observed ZrO_6 positions. These data are also shown graphically in Fig. 7 relative to values for an ideal structure.

Distortions of the V_2O_7 groups can be described by considering the deviation of the V—V vector from the threefold axis, the V—O—V bond angle and the torsion angle of the O_{Zr} atoms. In the ideal high-temperature structure all V—V vectors lie parallel to a threefold axis and the center of symmetry at the bridging atom requires that O_{Zr} atoms of the two vanadiums be perfectly staggered (*i.e.* 60° torsion angles). In the low-temperature structure V—V vectors deviate by up to 5.4° from the threefold axis and torsion angles in certain groups decrease by up to 21°. These angles are shown graphically in Fig. 3 and are tabulated in Table 5.

The above results all suggest that the low-temperature form of ZrV_2O_7 contains highly regular essentially undistorted polyhedra. Except for minor changes in V—O_V bond distances, the major structural changes involve rotations of these coupled polyhedra, resulting princi-

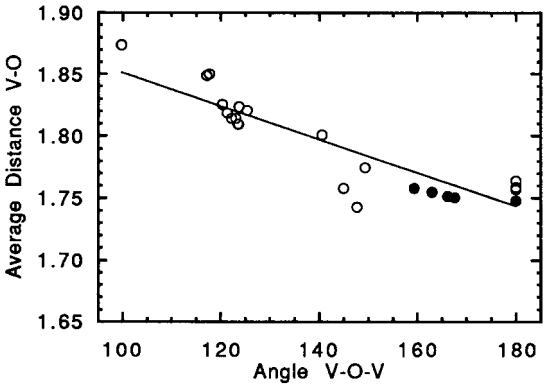

Fig. 6. Dependence of V—O distances on V—O—V bond angle for $M_2V_2O_7$ phases (open circles) and ZrV_2O_7 (closed circles).

Table 5. *Distortions of V_2O_7 groups*

V—V distances, V—O—V bond angles, tilt angle of V—V vector from threefold axis and maximum deviation of O—V—V—O torsion angle from 60° are given. Distances in Å.

V*n*—V*n*	V—O—V (°)	*d*(V—V) (Å)	Tilt (°)	Δ(Torsion) (°)
1-8	159.33	3.4590	3.18	7.05
2-7	162.92	3.4710	5.42	17.17
3-4	166.18	3.4780	1.09	8.21
5-6	167.58	3.4800	5.36	3.32
9-11	180.00	3.5020	0.00	21.01
10-10	180.00	3.4920	0.00	0.00

pally in changes in the Zr—O—V and V—O—V bond angles. It is interesting then to compare a purely geometrical model of the structure to the true structure. Distance least-squares modeling was performed in *CRYSTALS* (Watkin *et al.*, 1985) using average Zr—O bond distances of 2.072, $V—O_{Zr}$ 1.671 and $V—O_V$ 1.7545 Å (*i.e.* close to average values determined experimentally). Bond distances were restrained with an s.u. of 0.001 Å and bond angles with an s.u. of 0.1°. Using these parameters an 'ideal' structure with perfect polyhedra and 180° bond angles will result using a cell edge of 26.56 Å. Reducing the cell edge to 26.296 Å results in coupled rotations of these polyhedra. All such reductions in cell edge require, however, very minor distortions of the octahedral and/or tetrahedral bond distances and angles. The weights were chosen such that the relative distortions of distances and angles at a cell edge of 26.296 Å matched those observed experimentally (*i.e.* standard uncertainty of all metal–oxygen bond distances in the model ~0.005 Å, polyhedral bond angles ~0.5°).

Such a structure matched extremely closely that derived experimentally. The range of Zr—O—V bond angles was 145.6–174.6°. Tilts of the ZrO_6 octahedra (Table 4) are also very close to those observed. Average atomic shifts between the calculated and refined models were only 0.03 Å, with a maximum shift of 0.06 Å. As a final test, refinement of the calculated model with only a scale factor and an equated displacement parameter for each atomic type was performed. The *R* factor of R_F = 0.1194 compares with a value of 0.0645 for an isotropically refined structure.

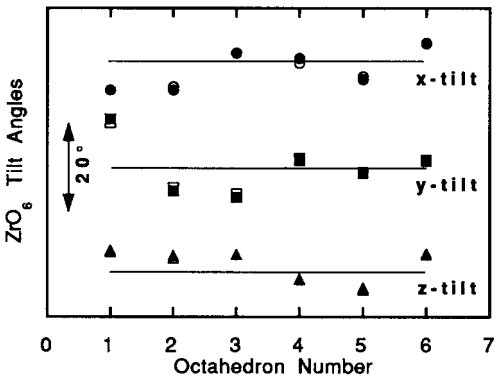

Fig. 7. Deviation of octahedral tilt angles from their high-temperature ideal values for the refined (closed symbols) and modeled (open symbols) structure. *x* tilts shown as circles, *y* tilts as squares, *z* tilts as triangles. Each horizontal line represents the zero for each individual tilt. The arrow represents a 20° range.

4. Conclusions

The work described here represents, we believe, the first definitive structural refinement of the superstructure of an AM_2O_7 phase. With no restraints imposed, a remarkably regular structure is obtained which contains essentially undistorted ZrO_6 octahedra and VO_4 tetrahedra. The coordination environments and hence calculated valences of all chemically equivalent atoms in the structure are essentially identical. The thermal motion of V—O—V bridging O atoms on the threefold axis is comparable to that of other bridging O atoms. ZrV_2O_7 undergoes two phase transitions between its high-temperature and room-temperature structure, which reduce the overall cell volume by destroying 26/27 of the translational symmetry elements. This allows four of the six V—O—V bridging groups to bend, whilst the remaining two remain fixed by symmetry at 180°. Further modeling of these phase transitions and a description of the intermediate (incommensurate) structure will be the subject of a forthcoming paper.

This work was supported through NSF grant No. DMR-9308530. Research was carried out in part at the National Synchrotron Light Source, Brookhaven National Laboratory, which is supported by the US Department of Energy, Division of Materials Sciences and Division of Chemical Sciences. We would like to thank Dr V. Korthuis for providing the single crystal used and Kemin Tan for assistance during the data collection.

References

Baerlocher, C., Hepp, A. & Meier, W. M. (1977). *DLS Software*. Institute of Crystallography and Petrology, Eidgenössiche Technische Hochschule, Switzerland.

Banks, E. & Sacks, R. (1982). *Mater. Res. Bull.* **17**, 1053–1055.

Buchanan, R. C. & Walter, G. W. (1983). *J. Electrochem. Soc. Solid State Sci. Technol.* **130**, 1905–1910.

Burdese, A. & Borlera, M. L. (1960). *Ann. Chim. (Rome)*, **50**, 1570–1583.

Burdese, A. & Borlera, M. L. (1963). *Ann. Chim. (Rome)*, **53**, 333–343.

Chaunac, M. (1971). *Bull. Soc. Chim. Fr.* pp. 424–429.

Fukuoka, H., Imoto, H. & Saito, T. (1995). *J. Solid State. Chem.* **119**, 98–106.

Gibbs, G. V., Downs, J. W. & Boisen, M. B. Jr (1994). *Silica Rev. Min.* **29**, 331–363.

Hagmann, L.-O. & Kierkegaard, P. (1969). *Acta Chem. Scand.* **23**, 327–328.

Haushalter, R. C. & Mundi, L. A. (1992). *Chem. Mater.* **4**, 31–48.
Huang, C. H., Knop, O., Othen, D. A., Woodhams, F. W. D. & Howie, R. A. (1975). *Can. J. Chem.* **53**, 79–91.
Hudalla, C., Eckert, H. & Dupree, R. (1996). *J. Phys. Chem.* **100**, 15986–15991.
Khosrovani, N. & Sleight, A. W. (1996). *Inorg. Chem.* **35**, 485–489.
Khosrovani, N., Sleight, A. W. & Vogt, T. (1997). *J. Solid State Chem.* **132**, 355–360.
Korthuis, V., Khosrovani, N., Sleight, A. W., Roberts, N., Dupree, R. & Warren, W. W. Jr (1995). *Chem. Mater.* **7**, 412–417.
Larson, A. C. (1970). *Crystallographic Computing*, edited by F. R. Ahmed, S. R. Hall & C. P. Huber, pp. 291–294. Copenhagen: Munksgaard.
Larson, A. C. & Von Dreele, R. B. (1994). *GSAS Software*. LANSCE, Los Alamos National Laboratory, USA.
Levi, G. R. & Peyronel, G. (1935). *Z. Kristallogr.* **92**, 190–209.
Liebau, F., Bissert, G. & Köppen, N. (1968). *Z. Anorg. Allg. Chem.* **359**, 113–129.
Minor, W. (1993). *XDISPLAYF Program*. Purdue University, USA.
Norby, P. (1996). Personal communication.
Otwinowski, Z. (1993). *Oscillation Data Reduction Program. Proceedings of the CCP4 Study Weekend: Data Collection and Processing*, compiled by L. Sawyer, N. Isaacs & S. Bailey, pp. 52–62. Daresbury Laboratory, England.
Oyetola, S., Verbaere, A., Guyomard, D., Crosnier, M. P., Piffard, Y. & Tournoux, M. (1991). *Eur. J. Solid State Chem.* **28**, 23–36.
Pascard, R., Chaunac, M. & Grison, E. (1971). *Bull. Soc. Chim. Fr.* pp. 429–435.
Peyronel, G. (1942). *Gazz. Chim. Ital.* **72**, 83–88.
Sanz, J., Iglesias, J. E., Solia, J., Loailla, E. R., Aranda, M. A. G. & Bruque, S. (1997). *Chem. Mater.* **9**, 996–1003.
Seo, D.-K. & Whangbo, M.-H. (1997). *J. Solid State Chem.* **129**, 160–163.
Tillmanns, E., Gebert, W. & Baur, W. H. (1973). *J. Solid State Chem.* **7**, 69–84.
Völlenke, H., Wittman, A. & Nowotny, H. (1963). *Monatsh. Chem.* **94**, 956–963.
Watkin, D. J., Carruthers, J. R. & Betteridge, P. W. (1985). *CRYSTALS User Guide*. Chemical Crystallography Laboratory, University of Oxford, England.
Withers, R. L., Evans, J. S. O., Hanson, J. & Sleight, A. W. (1998). *J. Solid State Chem.* **137**, 161–167.
Zah Letho, J. J., Oyetola, S., Verbaere, A., Taulelle, F. & Piffard, Y. (1994). *Eur. J. Solid State Chem.* **31**, 1009–1020.